GENERATION OF AERODYNAMICS VIA PHYSICS-BASED VIRTUAL FLIGHT SIMULATIONS

J. Sahu[*]
U.S. Army Research Laboratory
Aberdeen Proving Ground, Maryland 21005-5069

M. Costello
Georgia Institute of Technology
Atlanta, Georgia 30332

ABSTRACT

A method to efficiently generate a complete aerodynamic description for projectile flight dynamic modeling is described. At the core of the method is an unsteady, time accurate computational fluid dynamics simulation that is tightly coupled to a rigid projectile flight dynamic simulation. This coupled multidisciplinary technique allows "virtual fly-out" of projectiles on supercomputers, predicts the fight path of a projectile and all the associated unsteady free-flight aerodynamics in an integrated manner, and offers a new appraoch for generating a complete aerodynamic description consisting of both static and dynamic aerodynamic coefficients. A set of short time snippets of simulated projectile motion at different Mach numbers is computed and employed as baseline data. For each time snippet, aerodynamic forces and moments and the full rigid body state vector of the projectile are known. With time synchronized air loads and state vector information, aerodynamic coefficients can be estimated with a simple fitting procedure. By inspecting the condition number of the fitting matrix, it is straight forward to assess the suitability of the time history data to predict a selected set of aerodynamic coefficients.   The technique is exercised on a fin stabilized projectile with promising results.

1. INTRODUCTION

Understanding the aerodynamics of projectiles, rockets, and missiles is critical to the design of stable configurations and contributes significantly to the overall performance of weapon systems [1-3]. The prediction of aerodynamic coefficients for these weapon systems is essential in assessing the performance of new designs. Numerical simulations have the potential of greatly reducing design costs while providing a detailed understanding of the complex aerodynamics associated with each change. Improved computer technology and state-of-the-art numerical procedures now enable solutions to complex, three-dimensional (3-D) problems associated with projectile and missile aerodynamics. For maneuvering munitions, the effect of many new weapon control mechanisms being proposed such as deployable pins, pulsed flaps, microjets on flight dynamics is critical to the overall guided flight performance. Many of these mechanisms fall outside the range of conventional aerodynamic control and accurate well-validated tools for prediction of aerodynamic loads are desired.   These control mechanisms result in highly complex unsteady flow interactions and their accurate modeling during guided flight with active control is a major challenge [4-5].   Accurate numerical modeling of this unsteady aerodynamics has been found to be challenging both in terms of time-accurate solution techniques and computing resources required. As part of a DOD High Performance Computing Grand Challenge Project, our research work has been focused on the coupling of computational fluid dynamics CFD), rigid body dynamics (RBD) technique, and flight control systems (FCS) for simultaneous prediction of unsteady free-flight and control mechanism aerodynamics and the flight trajectory of projectiles. This multidisciplinary research has already resulted in a predictive capability that allows "virtual fly-out" of projectiles on supercomputers and predicts the fight path of a projectile and all the associated unsteady free-flight aerodynamics using coupled CFD/RBD techniques in an integrated manner [6]. The coupled CFD/RBD or virtual fly-out approach offers an ideal way to rapidly compute the aerodynamic coefficients (both static and dynamic). This new method of efficiently generating a complete aerodynamic description for projectile flight dynamic modeling is the subject of study here.

Computation time for accurate coupled CFD/RBD simulation remains relatively high and does not currently represent a practical method for typical flight dynamic analysis such as impact point statistics circular error probable (CEP) computation where thousands of fly outs are required. Furthermore, this type of analysis does not allow the same level of understanding of the inherent underlying dynamics of the system that rigid body dynamic analysis using aerodynamic coefficients yields. However, the coupled CFD/RBD approach does offer an indirect way to rapidly compute the aerodynamic coefficients needed for rigid 6 degree-of-freedom (6-DOF) simulation.   During a time-accurate CFD/RBD simulation, aerodynamic forces and moments and the full rigid body state vector of the projectile are generated at each time step in the simulation [6]. This means that

Report Documentation Page		Form Approved OMB No. 0704-0188

1. REPORT DATE **DEC 2008**	2. REPORT TYPE **N/A**	3. DATES COVERED **-**

4. TITLE AND SUBTITLE	5a. CONTRACT NUMBER
Generation Of Aerodynamics Via Physics-Based Virtual Flight Simulations	5b. GRANT NUMBER
	5c. PROGRAM ELEMENT NUMBER
6. AUTHOR(S)	5d. PROJECT NUMBER
	5e. TASK NUMBER
	5f. WORK UNIT NUMBER

7. PERFORMING ORGANIZATION NAME(S) AND ADDRESS(ES) **U.S. Army Research Laboratory Aberdeen Proving Ground, Maryland 21005-5069**	8. PERFORMING ORGANIZATION REPORT NUMBER

9. SPONSORING/MONITORING AGENCY NAME(S) AND ADDRESS(ES)	10. SPONSOR/MONITOR'S ACRONYM(S)
	11. SPONSOR/MONITOR'S REPORT NUMBER(S)

12. DISTRIBUTION/AVAILABILITY STATEMENT
Approved for public release, distribution unlimited

13. SUPPLEMENTARY NOTES
See also ADM002187. Proceedings of the Army Science Conference (26th) Held in Orlando, Florida on 1-4 December 2008, The original document contains color images.

14. ABSTRACT

15. SUBJECT TERMS

16. SECURITY CLASSIFICATION OF:			17. LIMITATION OF ABSTRACT	18. NUMBER OF PAGES	19a. NAME OF RESPONSIBLE PERSON
a. REPORT **unclassified**	b. ABSTRACT **unclassified**	c. THIS PAGE **unclassified**	**UU**	**8**	

aerodynamic forces, aerodynamic moments, position of the mass center, body orientation, translational velocity, and angular velocity of the projectile are all known at the same time instant. With time synchronized air load and state vector information, the aerodynamic coefficients can be estimated with a simple fitting procedure.

This paper creates a method to efficiently generate a complete aerodynamic model for a projectile in atmospheric flight using four short time histories at each Mach number of interest with an advanced time accurate CFD/RBD simulation. The technique is exercised on example CFD/RBD data obtained on a small fin stabilized projectile.

2. NUMERICAL PROCEDURE

A real time-accurate approach is used in the present work. This approach requires that the six-degrees-of-freedom body dynamics be computed at each repetition of the fluid flow solver. In three-dimensional space, a rigid object has six degrees of freedom: three translations and three rotations. The six-degree-of-freedom code computes linear and angular velocities as well as the orientation of the projectile, which are used as input to the computational fluid dynamics code. In turn, the aerodynamic forces and moments obtained from the flow solver are used to solve the 6-dof body dynamics before moving on to the next time step. This procedure allows one to perform real-time multidisciplinary-coupled computational fluid dynamics/rigid body aerodynamics computations for the partial or entire flight trajectory of a complex guided projectile system.

The CFD capability used here solves the Navier Stokes equations [7-9] and incorporates advanced boundary conditions and grid motion capabilities [6]. The present numerical study is a direct extension of that research for generation of a complete aerodynamic model using very short virtual fly-outs. These fvirtual fly-outs involve numerical simulation of the actual fight paths of the projectile using coupled time-accurate CFD/RBD techniques. The complete set of 3-D time-dependent Navier-Stokes equations is solved in a time-accurate manner for simulations of actual flights. The basic numerical framework in the code contains unified-grid, unified-physics, and unified-computing features. The user is referred to these references for details of the basic numerical framework. The 3-D time-dependent Reynolds-averaged Navier-Stokes (RANS) equations are solved using the finite volume method [7]:

$$\frac{\partial}{\partial t} \int_V \mathbf{W} dV + \oint [\mathbf{F} - \mathbf{G}] \cdot dA = \int_V \mathbf{H} dV \qquad (1)$$

where W is the vector of conservative variables, F and G are the inviscid and viscous flux vectors, respectively, H is the vector of source terms, V is the cell volume, and A is the surface area of the cell face.

Second-order discretization was used for the flow variables and the turbulent viscosity equation. The turbulence closure is based on topology-parameter-free formulations. Two-equation [9] and higher order hybrid RANS/LES [10] turbulence models are available for computation of turbulent flows. The hybrid RANS/LES approach is well suited to the simulation of unsteady flows and contains no additional empirical constants beyond those appearing in the original RANS and LES sub-grid models. With this method a regular RANS-type grid is used except in isolated flow regions where denser, LES-type mesh is used to resolve critical unsteady flow features. The hybrid model transitions smoothly between an LES calculation and a cubic k-ε model, depending on grid fineness. For computations of unsteady flow fields that are of interest here, dual time-stepping was used to achieve the desired time-accuracy. In addition, unsteady RANS method was used in the present study for computation of the unsteady flow field associated with supersonic free-flights.

An unique feature of the present coupled approach is the full grid motion capability that allows the grid to move translate and rotate as the projectile flies down the rage, since the grid velocity is assigned to each mesh point. To account for rigid body dynamics, the grid point velocities are set as if the grid is attached to the rigid body with six degrees of freedom (6 DOF). As shown schematically in Figure 1, the six degrees of freedom comprise of the three spatial coordinates (x,y,z) and the
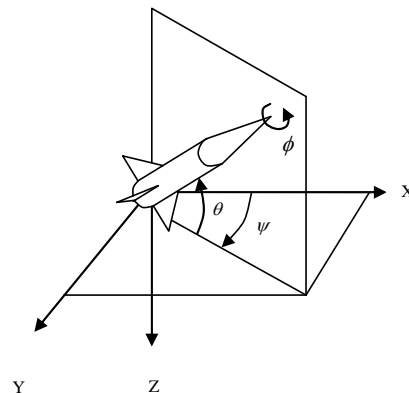

Figure 1. Rigid Body Dynamics Schematic.

three Euler angles, roll, pitch, and yaw (φ, Φ, Ψ). For the rigid body dynamics, the coupling refers to the interaction between the aerodynamic forces/moments and the dynamic response of the projectile/body to these forces and moments. The forces and moments are computed

every CFD time step and transferred to a 6DOF module which computes the body's response to the forces and moments. The response is converted into translational and rotational accelerations that are integrated to obtain translational and rotational velocities and integrated once more to obtain linear position and angular orientation. The grid point locations and grid point velocities are the set from the dynamic response. Both CFD and RBD computations are performed at every time step in a fully coupled manner.

The projectile in the coupled CFD/RBD simulation along with its grid moves and rotates as the projectile flies downrange. Grid velocity is assigned to each mesh point. This general capability can be tailored for many specific situations. For example, the grid point velocities can be specified to correspond to a spinning projectile. In this case, the grid speeds are assigned as if the grid is attached to the projectile and spinning with it. Similarly, to account for rigid body dynamics, the grid point velocities can be set as if the grid is attached to the rigid body with six degrees of freedom. As shown in Figure 1, the 6-DOF comprises of the inertial position components of the projectile mass center (x, y, z) and the three standard Euler angles (ϕ, θ, ψ), roll angle, pitch angle, and yaw angle, respectively.

In order to properly initialize the CFD simulation, two modes of operation for the CFD code are utilized, namely, an uncoupled and a coupled mode. The uncoupled mode is used to initialize the CFD flow solution while the coupled mode represents the final time-accurate coupled CFD/RBD solution. In the uncoupled mode, the rigid body dynamics are specified. The uncoupled mode begins with a computation performed in a "steady state mode" with the grid velocities prescribed to account for the proper initial position (x_0, y_0, z_0), orientation (ϕ_0, θ_0, ψ_0), and translational velocity (u_0, v_0, w_0) components of the complete set of initial conditions to be prescribed. After the steady state solution is converged, the initial spin rate (p_0) is included and a new quasi-steady state solution is obtained using time-accurate CFD. A sufficient number of time steps are performed so that the angular orientation for the spin axis corresponds to the prescribed initial conditions. This quasi-steady state flow solution is the starting point for the time-accurate coupled solution. For the coupled solution, the mesh is translated back to the desired initial position (x_0, y_0, z_0) and the remaining angular velocity initial conditions (q_0, r_0) are then added. In the coupled mode, the aerodynamic forces and moments are passed to the RBD simulation which propagates the rigid state of the projectile forward in time.

3. FLIGHT DYNAMIC PROJECTILE AERODYNAMIC MODEL

The applied loads in the standard 6-DOF equations of motion contain contributions from projectile weight and body aerodynamic forces and moments as shown below.

$$
\begin{Bmatrix} X \\ Y \\ Z \end{Bmatrix} = W \begin{Bmatrix} -s_\theta \\ s_\phi c_\theta \\ c_\phi c_\theta \end{Bmatrix} - \frac{\pi}{8} \rho V^2 D^2 \begin{Bmatrix} C_{X0} + C_{X2}(v^2 + w^2)/V^2 \\ C_{NA} v/V - \frac{pD}{2V} C_{YPA} w/V \\ C_{NA} w/V + \frac{pD}{2V} C_{YPA} v/V \end{Bmatrix} \quad (2)
$$

$$
\begin{Bmatrix} L \\ M \\ N \end{Bmatrix} = \frac{\pi}{8} \rho V^2 D^3 \begin{Bmatrix} C_{LDD} + \frac{pD}{2V} C_{LP} \\ C_{MA} \frac{w}{V} + \frac{qD}{2V} C_{MQ} + \frac{pD}{2V} C_{NPA} \frac{v}{V} \\ -C_{MA} \frac{v}{V} + \frac{rD}{2V} C_{MQ} + \frac{pD}{2V} C_{NPA} \frac{w}{V} \end{Bmatrix} \quad (3)
$$

In Equations 2 and 3, we use the shorthand notation $s_\alpha = \sin(\alpha)$, $c_\alpha = \cos(\alpha)$, and $t_\alpha = \tan(\alpha)$. Note that the total applied force components (X, Y, Z) and moment components (L, M, N) contain contributions from weight and aerodynamics. The aerodynamic portion of the applied loads in Equations 2 and 3 is computed using the CFD simulation and passed to the rigid body dynamic simulation.

The terms containing C_{YPA} constitute the Magnus air load acting at the Magnus center of pressure while the terms containing C_{X0}, C_{X2}, C_{NA} define the steady load acting at the center of pressure. The externally applied moment about the projectile mass center is composed of an unsteady aerodynamic moment along with terms due to the fact that the center of pressure and center of Magnus are not located at the mass center. The terms involving C_{MA} accounts for the center of pressure being located off the mass center while the terms involving C_{NPA} accounts for the center of Magnus being located off the mass center. The aerodynamic coefficients are all a function of local Mach number which are typically handled through a table look-up scheme in projectile flight simulation codes. The aerodynamic model presented in Equations 2 and 3 is the standard aerodynamic expansion for symmetric projectiles.

4. PROJECTILE AERODYNAMIC COEFFICIENT ESTIMATION (PACE)

The time-accurate coupled CFD/RBD simulation provides a full flow solution including the aerodynamic

portion of the total applied force and moment (X, Y, Z, L, M, N) along with the full state of the rigid projectile ($x, y, z, \phi, \theta, \psi, u, v, w, p, q, r$) at every time step in the solution for each time snippet. Given a set of n short time histories (snippets) that each contain m time points yields a total of $h = m * n$ time history data points for use in estimating the aerodynamic coefficients: $C_{X0}, C_{X2}, C_{NA}, C_{YPA},$ $C_{LDD}, C_{LP}, C_{MA}, C_{MQ}, C_{NPA}$. Note that for fin-stabilized projectile configurations, the Magnus force and moment are usually sufficiently small so that C_{YPA} and C_{NPA} are set to zero and removed from the fitting procedure to be described below.

Equations 2 and 3 represent the applied air loads on the projectile expressed in the projectile body frame. Computation of the aerodynamic coefficients is aided by transforming these equations to the instantaneous aerodynamic angle of attack reference frame that rotates the projectile body frame about the $\vec{I}_B$ axis by the angle $\gamma = \tan^{-1}(w/v)$.

$$-\frac{8}{\pi\rho V^2 D^2}\begin{bmatrix}1 & 0 & 0\\0 & c_\gamma & s_\gamma\\0 & -s_\gamma & c_\gamma\end{bmatrix}\left(\begin{Bmatrix}X\\Y\\Z\end{Bmatrix} - W\begin{Bmatrix}-s_\theta\\s_\phi c_\theta\\c_\phi c_\theta\end{Bmatrix}\right) = \begin{Bmatrix}C_{X0} + C_{X2}(v^2+w^2)/V^2\\C_{NA}\dfrac{\sqrt{v^2+w^2}}{V}\\\dfrac{pD}{2V}\dfrac{\sqrt{v^2+w^2}}{V}C_{YPA}\end{Bmatrix} \quad (4)$$

$$\frac{8}{\pi\rho V^2 D^3}\begin{bmatrix}1 & 0 & 0\\0 & c_\gamma & s_\gamma\\0 & -s_\gamma & c_\gamma\end{bmatrix}\begin{Bmatrix}L\\M\\N\end{Bmatrix} = \begin{Bmatrix}C_{LDD} + \dfrac{pD}{2V}C_{LP}\\\dfrac{(vq+wr)D}{2\sqrt{v^2+w^2}V}C_{MQ} + \dfrac{pD}{2V}\dfrac{\sqrt{v^2+w^2}}{V}C_{NPA}\\\dfrac{(vr-wq)D}{2\sqrt{v^2+w^2}V}C_{MQ} - \dfrac{\sqrt{v^2+w^2}}{V}C_{MA}\end{Bmatrix} \quad (5)$$

Each time history data point provides a total of six equations given by the components of Equations 4 and 5. The first component of Equation 4 is gathered together for all time history data points to form Equation 6. Likewise, the second and third components of Equation 4 and all three terms of the Equation 5 are used to generate additional equations for the aerodynamic coefficients to be solved. Subscripts on the projectile state vector and aerodynamics force and moment components represent the time history data point.

$$\begin{bmatrix}1 & (v_1^2+w_1^2)/V_1^2\\\vdots & \vdots\\1 & (v_h^2+w_h^2)/V_h^2\end{bmatrix}\begin{Bmatrix}C_{X0}\\C_{X2}\end{Bmatrix} = \begin{Bmatrix}-\dfrac{8}{\pi\rho V_1^2 D^2}(X_1 + W\sin\theta_1)\\\vdots\\-\dfrac{8}{\pi\rho V_h^2 D^2}(X_h + W\sin\theta_h)\end{Bmatrix} \quad (6)$$

These new equations (Equation 6 and other similar equations not shown here) represent a set of five

uncoupled problems to solve for the different aerodynamic coefficients. To estimate the aerodynamic coefficients near a particular Mach number, a set of n time accurate coupled CFD/RBD simulations are created over a relatively short time period. Since an individual time snippet is over a short time period where the projectile state variables don't change appreciably, it is critical that initial conditions for the different time snippet be selected in an informed way so that the rank of each of the fitting matrices above is maximal. Properties of the fitting matrices above, such as the rank or condition number, can be used as an indicator of the suitability of the CFD/RBD simulation data to estimate the aerodynamic coefficients at the target Mach number. Equation 6 is employed to estimate the zero yaw drag coefficient (C_{X0}) and the yaw drag coefficient (C_{X2}). To minimize the condition number of this fitting matrix, both low and high aerodynamic angle of attack time snippets are required. Similarly, another equation is used to compute the normal force coefficient (C_{NA}) and it requires time history data with a nonzero aerodynamic angle of attack. Another equation generated from Equation 4 is used to compute the Magnus force coefficient (C_{YPA}) and it requires time history data with both low and high roll rate and aerodynamic angle of attack. Equation 5 is employed to estimate the fin cant roll coefficient (C_{LDD}) along with the roll damping coefficient (C_{LP}). To minimize the condition number of this fitting matrix, both low and high roll rate time snippets are required. The pitching moment coefficient (C_{MA}), the pitch damping coefficient (C_{MQ}), and the Magnus moment coefficient (C_{NPA}) are all estimated using similar procedure. For successful estimation of these coefficients, time history data with both low and high roll rate and aerodynamic angle of attack as well as low and high aerodynamic angle of attack are required. To meet the requirements for successful estimation of all five sets of aerodynamic coefficients, four time snippets are used all with different initial conditions. This set of time snippets contain a diverse set of initial conditions; Case 1: zero aerodynamic angle of attack and zero angular rates; Case 2: high angle of attack (20°) and zero angular rates; Case 3: low angle of attack (5°), high roll rate (377 rad/s) with other angular rates zero ; Case 4: zero angle of attack, high pitch rate (-10 rad/s) with other angular rates zero.

For flight dynamic simulation, aerodynamic coefficients are required at a set of Mach numbers that covers the intended spectrum of flight conditions for the round. If aerodynamic coefficients are estimated at k different Mach numbers then a total of $l = k * n$ CFD/RBD time snippets must be generated to construct

the entire aerodynamic database for flight simulation purposes.

5. RESULTS

Numerical simulations of the short virtual fly-outs have been carried out at ARL Major Shared Resource Center using 64 processors on a Linux Cluster as part of a Grand Challenge Project. Results obtained from a comutational validation study at a given supersonic speed are presented first. The same coupled CFD/RBD technique is then extended to other Mach numbers in the supersonic speed regime and short CFD/RBD virtual fly-outs are performed to generate aerodynamic coefficients at these speeds.

5.1 Validation of CFD/RBD Virtual Fly-Out in a Supersonic Flight

As part of a validation of the coupled Navier-Stokes and 6-DOF method, computed results have been obtained at an initial supersonic speed, M = 3.0 and angle of attack, α = -5° for a finned projectile using an unstructured time-accurate Navier-Stokes computational technique that includes grid motion capabilities. In addition, the projectile in the coupled CFD/RBD simulation actually moved along with its grid as it flew downrange.

The supersonic projectile modeled in this study is an ogive-cylinder-finned configuration (see Figure 2). The length of the projectile is 121 mm and the diameter is 13mm. The ogive nose is 98.6 mm long and the afterbody has a 22.3 mm, 2.5° boat-tail. Four fins are located on the back end of the projectile. Each fin is 22.3 mm long and 1.02 mm thick. An unstructured computational mesh (see Figure 3) was generated for this projectile. In general, most of the grid points are clustered in the boundary-layer and afterbody fin regions.
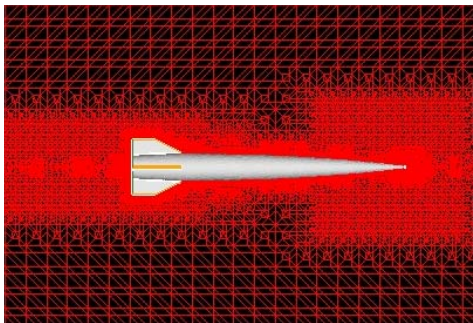

Figure 2. Supersonic finned projectile.

Figure 3. Unstructured mesh near the finned body.

The first spacing away from the wall was selected to yield a y+ value of 1.0 in each cases. The unstructured mesh was generated using the Multipurpose Intelligent Meshing Environment (MIME) grid-generation software recently developed by Metacomp Technologies.

The total aerodynamic forces and moments were used for the "virtual" fly-outs of the projectiles. Numerical computations were made for the generic finned projectile configuration at an initial velocity of 1032 m/s. The initial angle of attack was, α = 4.9° and initial spin rate was 2500 rad/s. Figure 4 shows the computed pressure contours at a given time or at a given location in the trajectory. It clearly shows the orientation of the body at that instant in time and the resulting asymmetric flow field due to the body at angle of attack. The orientation of the projectile of course changes from one instant in time to another as the projectile flies down range. Figure 5 shows the variation of the Euler pitch angle with distance
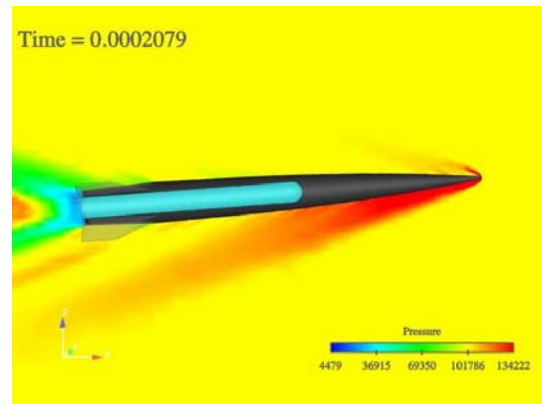

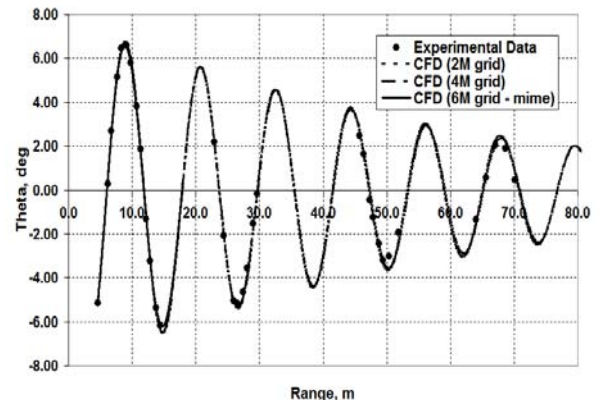Figure 4. Computed pressure contours.

Figure 5. Effect of mesh size on the Euler pitch angle.

traveled. As seen in this figure, both the amplitude and frequency in the Euler angle variation are predicted very well by the computed results and match extremely well with the data from the flight tests. One can also clearly

see that the amplitude damps out as the projectile flies down range i.e. with the increasing x-distance. Although not shown here, similar behavior is observed with the Euler yaw angle and it damps out with the increasing x-distance. Computed results again compare very well with the measured data from the flight tests. As stated earlier, different computational meshes were used to obtain the numerical results. Grid sizes varied from 2 to 6 million total number of points. The effect of the grid sizes on the computed Euler pitch angle is also shown in Figure 5. As seen here, these computed results are grid-independent; the computed pitch angles obtained with 4 and 6 million mesh are essentially the same as those results obtained with the 2 million point mesh. In all our subsequent computations, the 4 million grid point mesh has been used. Additional validation results showing other state variables and more details can be found in Reference 6.

5.2 Short Virtual Fly-Outs at different Supersonic Mach numbers

Computed results obtained have been obtained from the virtual fly-out simulations for the four short time snippets described earlier. These simulations correspond to different initial conditions and are performed at each supersonic Mach number considered here from Mach = 1.5 to 4.0. The projectile state trajectories for each of the four time snippets are computed. Each time snippet is 0.023 sec and contains 50 points, leading to an average output time step of 0.0004. These four snippets create time history data at low and high angle of attack, roll rate, and pitch rate needed for accurate aerodynamic coefficient estimation. Notice that cases 2 and 3 have notably more drag down due to the high angle of attack launch conditions. Case 3 is launched with relatively high roll rate compared to all other cases. Significant oscillations in Euler pitch angle and therefore, the total angle of attack (see Figure 6) are created. As seen in Figure 6, the angle of attack decreases with time for cases 2 and 3. Aerodynamic forces and moments are obtained
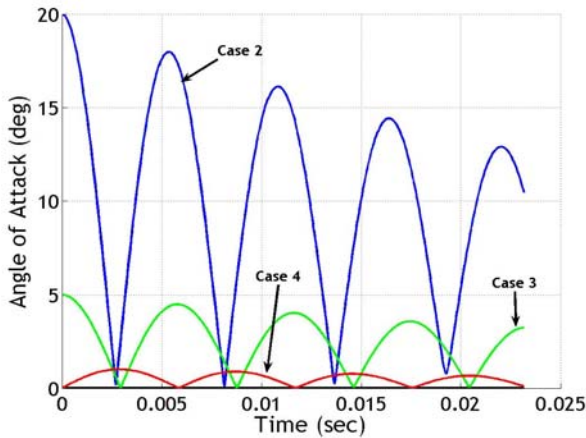
in the local angle of attack reference frame defined above for cases 1, 3, and 4 since these cases are the primary cases used to estimate the coefficients. Figures 7 and 8 show a few representative results for the side force and the yawing moment, respectively. Although not shown here, for moderately high angles of attack (case 3), the estimated data also oscillates with a much higher amplitude than the CFD/RBD data indicating that CX2 is estimated larger than the CFD/RBD suggests. The normal force time snippets agree well between the
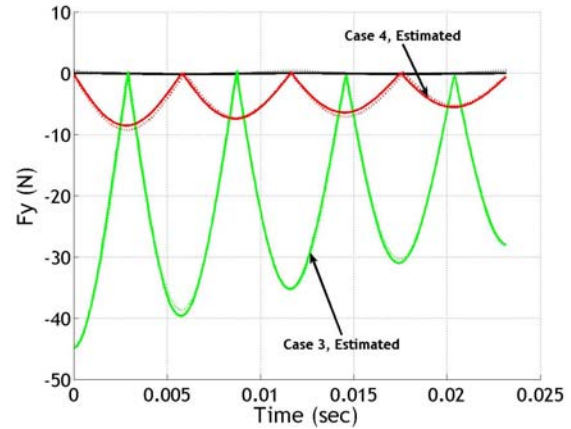

Figure 7. Estimated (Dashed) and CFD/RBD (Solid) Normal Force versus Time.
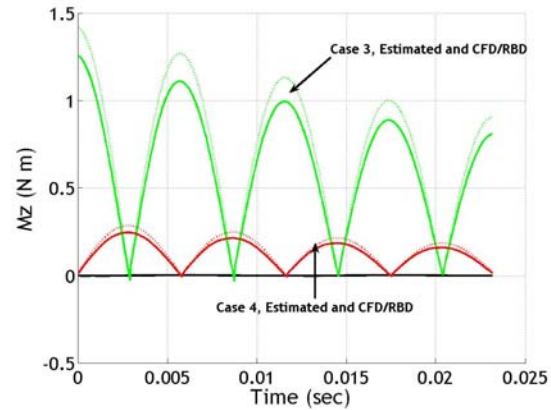

Figure 8. Estimated (Dashed) and CFD/RBD (Solid) Yawing Moment versus Time.

CFD/RBD and estimated data for all time snippets. For the example finned projectile, side force and out-of-plane moment are generally small due to a negligibly small Magnus force and moment. The CFD/RBD and estimated data agree reasonably well, but certainly do not overlay one another (see Figure 7). The only time snippet that creates notable rolling moment is case 3 which is launched with an initial roll rate of 377 rad/sec. The in-plane moment (Mz) agrees reasonably well for both the CFD/RBD and estimated data (see Figure 8). These

Figure 6. Aerodynamic Angle of Attack for the Time Snippets

results shown are typical for all Mach numbers considered in this study. The overall observation from the data is that the estimated aerodynamic model fits the CFD/RBD data reasonably well.

CFD/RBD data was generated at six different Mach numbers ranging from 1.5 to 4.0. The estimation algorithm discussed above was used to compute a complete set of aerodynamic coefficients across this Mach range. These results are provided in Figures 9 throuth 13 for the aerodynamic coefficients. The steady aerodynamic coefficients are smooth and follow typical trends for variation in Mach number. Pitch damping decreases with Mach number as would be expected for a fin stabilized projectile beyond Mach 1.0. Roll damping steadily increases until Mach 4.0 when it drops off a little. The projectile investigated in this paper has been fired in a spark range at various supersonic speeds with aerodynamic coefficients obtained via conventional aerodynamic range reduction. Figures 9 through 13 also show comparisons of aerodynamic coefficients obtained
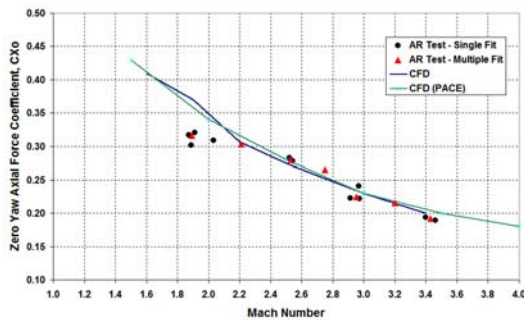

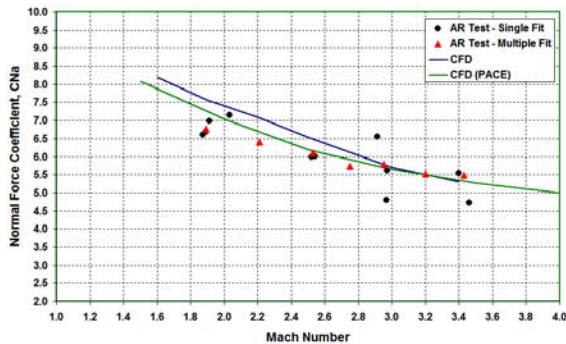Figure 9. Zero-yaw drag coefficient vs. Mach number.

Figure 10. Normal force coefficient vs. Mach number.

from spark range testing and subsequent coefficients obtained using the method described here. Computed results are compared with the data derived from free flight tests for the same projectile configuration using single and

multiple fits. Also shown in these comparisons are some of the aerodynamic coefficients obtained using conventional CFD techniques. Notice that most aerodynamic coefficients such as CX0, CNA, and CMA are in reasonably good agreement with spark range reduced data except for the drag at lower Mach numbers around Mach = 1.9 and the pictching moment at higher
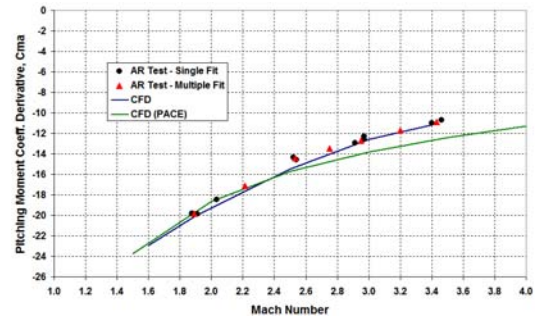

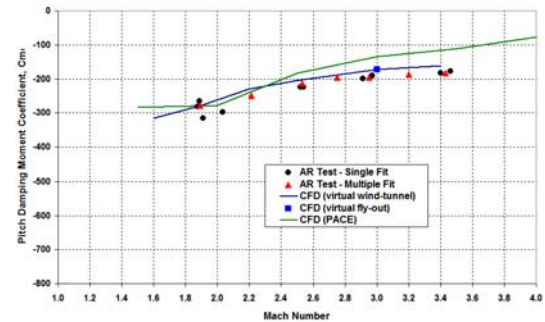Figure 11. Pitching moment coefficient vs. Mach number.

Figure 12. Pitch-damping moment coefficient vs. Mach number.

Mach numbers greater than 3.0. The difference between the these static aerodynamic coefficients obtained using PACE procedure and those obtained using conventional CFD techniques is generally small (see Figures 9-11). The CFD PACE procedure underpredicts the pitching moment coefficient by about 10-15% at Mach numbers higher than 3.0. The dynamic derivatives (the pitch-damping moment and the roll damping moment coefficients) are shown in Figures 12 and 13, respectively. Both the data and computed CFD results show similar trends. Comparison of the computed dynamic derivatives using PACE with the data show a slightly better agreement at lower Mach numbers. The discrepancy is larger at higher Mach numbers especially as seen in the pich-damping moment coefficient plot in Figure 12. In general, with the exception of CMQ, aerodynamic coefficients are nearly estimated to within the accuracy that can be expected from a spark range test firing

between two sets of firings. The relatively larger errors in CMQ are more than likely due to the set of initial conditions that create a large condition number for the fitting matrix.
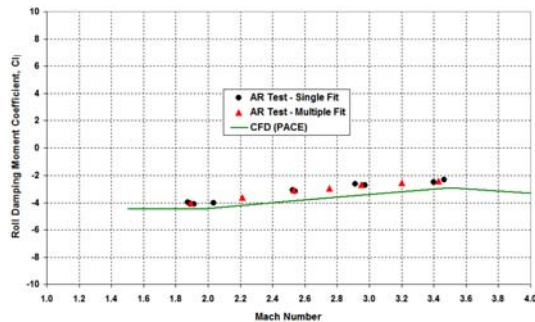

Figure 13. Roll damping moment coefficient vs. Mach number.

6. SUMMARY

Using a time accurate computational fluid dynamics simulation that is tightly coupled to a rigid body dynamics simulation, a method to efficiently generate a complete aerodynamic description for projectile flight dynamic modeling is described. A set of n short time snippets of simulated projectile motion at m different Mach numbers is computed and employed as baseline data. The combined CFD/RBD analysis computes time synchronized air loads and projectile state vector information, leading to a straight forward fitting procedure to obtain the aerodynamic coefficients. The estimation procedure decouples into five sub-problems that are each solved via linear least squares. The method has been applied to a supersonic finned projectile. A comparison of spark range obtained aerodynamic coefficients with the estimation method presented here exhibits generally good agreement within 10-15% for CX0, CNA, and CMA. A large discrpancey exists between the CMQ predicted by the PACE procedure and the test data. The PACE predicted aerodynamic coefficients are generally in good agreement with the aerodynamic coefficients computed using conventional CFD techniques except for CMQ at higher Mach numbers greater than 3.0. This technique reported here provides a promising new means for the CFD analyst to predict aerodynamic coefficients for flight dynamic simulation purposes. It can easily be extended to flight dynamic modeling of different control effectors provided accurate CFD/RBD time simulation is possible and an aerodynamic coefficient expansion is defined which includes the effect of the control mechanism. Further study is planned to improve the accuracy of the estimation procedure especially for the pitch-damping moment coefficient.

REFERENCES

1. Sahu, J., K. R. Heavey, and C. J. Nietubicz, "Time-Dependent Navier-Stokes Computations for Submunitions in Relative Motion." 6th International Symposium on Computational Fluid Dynamics, Lake Tahoe, NV, September 1995.

2. Sturek, W. B., Nietubicz, C. J, Sahu, J., Weinacht, P., "Applications of Computational Fluid Dynamics to the Aerodynamics of Army Projectiles, *Journal of Spacecraft and Rockets*, Vol 31, No 2, pp 186-199, 1994.

3. Meakin, R. L., "Computations of the Unsteady Flow About a Generic Wing/Pylon/Finned-Store Configuration." AIAA 92-4568-CP, August 1992.

4. Smith B. L., and A. Glezer, "The Formation and Evolution of Synthetic Jets." Journal of Physics of Fluids, vol. 10, No. 9, September 1998.

5. Davis, S. A. and Glezer, A., "The Manipulation of Large- and Small-Scales in Coaxial Jets using Synthetic Jet Actuators", AIAA Paper No. 2000-0403, January 2000

6. Sahu, J., "Time-Accurate Numerical Prediction of Free-Flight Aerodynamics of a Finned Projectile," AIAA-2005-5817, AIAA Atmospheric Flight Mechanics Conference, San Francisco, California, 2005.

7. Peroomian, O., S. Chakravarthy, and U. Goldberg, "A 'Grid-Transparent' Methodology for CFD." AIAA Paper 97-07245, 1997.

8. Peroomian, O., S. Chakravarthy, S. Palaniswamy, and U. Goldberg, "Convergence Acceleration for Unified-Grid Formulation Using Preconditioned Implicit Relaxation." AIAA Paper 98-0116, 1998.

9. Goldberg, U. C., O. Peroomian, and S. Chakravarthy, "A Wall-Distance-Free K-E Model With Enhanced Near-Wall Treatment." ASME Journal of Fluids Engineering, Vol. 120, pp. 457-462, 1998.

10. Batten, P., U. Goldberg and S. Chakravarthy, "Sub-grid Turbulence Modeling for Unsteady Flow with Acoustic Resonance", AIAA Paper 00-0473, 38th AIAA Aerospace Sciences Meeting, Reno, NV, January 2000.

11. Wayne H., "Private communications", Arrow Tech Associates, South Burlington, VT, June 2008.